Institute of Paper Science and Technology
Atlanta, Georgia

IPST Technical Paper Series Number 635

New Measures for Maximizing Ink Particle Removal in a Flotation Cell

T.J. Heindel and F. Bloom

January 1997

Submitted to
1997 TAPPI Recycling Symposium
Chicago, Illinois
April 14–16, 1997

INSTITUTE OF PAPER SCIENCE AND TECHNOLOGY
PURPOSE AND MISSIONS

The Institute of Paper Science and Technology is a unique organization whose charitable, educational, and scientific purpose evolves from the singular relationship between the Institute and the pulp and paper industry which has existed since 1929. The purpose of the Institute is fulfilled through three missions, which are:

- to provide high quality students with a multidisciplinary graduate educational experience which is of the highest standard of excellence recognized by the national academic community and which enables them to perform to their maximum potential in a society with a technological base; and
- to sustain an international position of leadership in dynamic scientific research which is participated in by both students and faculty and which is focused on areas of significance to the pulp and paper industry; and
- to contribute to the economic and technical well-being of the nation through innovative educational, informational, and technical services.

ACCREDITATION

The Institute of Paper Science and Technology is accredited by the Commission on Colleges of the Southern Association of Colleges and Schools to award the Master of Science and Doctor of Philosophy degrees.

NOTICE AND DISCLAIMER

The Institute of Paper Science and Technology (IPST) has provided a high standard of professional service and has put forth its best efforts within the time and funds available for this project. The information and conclusions are advisory and are intended only for internal use by any company who may receive this report. Each company must decide for itself the best approach to solving any problems it may have and how, or whether, this reported information should be considered in its approach.

IPST does not recommend particular products, procedures, materials, or service. These are included only in the interest of completeness within a laboratory context and budgetary constraint. Actual products, procedures, materials, and services used may differ and are peculiar to the operations of each company.

In no event shall IPST or its employees and agents have any obligation or liability for damages including, but not limited to, consequential damages arising out of or in connection with any company's use of or inability to use the reported information. IPST provides no warranty or guaranty of results.

NEW MEASURES FOR MAXIMIZING INK PARTICLE REMOVAL IN A FLOTATION CELL

Theodore J. Heindel
Assistant Professor
Engineering and Paper
Materials Division
Institute of Paper Science
and Technology
Atlanta, GA 30318

Frederick Bloom
Professor
Department of Mathematical
Sciences
Northern Illinois University
DeKalb, IL 60115

ABSTRACT

A population balance-type model of the flotation deinking process has been developed using two kinetic constants, which are functions of the microprocesses involved in flotation. These microprocesses are themselves functions of system parameters such as bubble and particle physical properties (e.g., diameter, density), fluid properties (e.g., viscosity, surface tension), and system properties (e.g., turbulent energy density, number of particles). The first kinetic constant, k_1, governs the overall probability that a free ink particle will successfully be intercepted by and adhere to an air bubble rising through a flotation cell, thereby accounting for the death of free particles in the unit cell. The second kinetic constant, k_2, addresses the probability that a bubble/ink particle aggregate will become unstable and split to yield a "new" free ink particle, which addresses the birth of free ink particles in the unit cell.

Model results have been used to identify three flotation cell performance parameters: (1) flotation efficiency as a function of time, (2) flotation efficiency for a given time period, and (3) the time it takes to reduce the number of free particles by a given amount. Selected predictions of these performance measures will be presented for a wide range of system parameters.

KEY WORDS:
population model, kinetic constants, microprocess probability, flotation cell, flotation efficiency

INTRODUCTION

In this paper, a simple mathematical model of the flotation deinking process, which was formulated by the authors in [1, 2], will be briefly reviewed and then used to construct two new, practical measures related to maximizing ink particle removal in a typical flotation cell.

In flotation deinking, air bubbles rise through agitated liquid tanks containing suspended cellulose pulp and contaminant particles and preferentially attach to hydrophobized contaminant and ink particles. These particles are, subsequently, transported to a froth layer where they may be easily removed. Although flotation cell designs may vary with respect to their geometry, flow configurations, and operating parameters, they all operate on similar principles and incorporate the fundamental processes of pulp aeration, mixing to maximize bubble/particle interaction, and separation of bubble/particle aggregates from the bulk mixture. Detailed descriptions of flotation cell operation can be found in the review articles [3, 4].

The prevalent viewpoint that has been taken in modeling the overall flotation separation process is that it is a multi-stage probability process consisting of a sequence of microprocesses with associated probability measures. This sequence includes the approach of a particle to an air bubble, the subsequent interception of that particle by the bubble, the sliding of the particle along the surface of the thin liquid film that separates the particle from the bubble, film rupture, the subsequent formation of a three-phase contact between the bubble, particle, and film, and the stabilization of the bubble/particle aggregate (with its subsequent transport to the froth layer for removal from the flotation cell).

Probability measures, which are associated with some of the elementary microprocesses referenced above, have appeared in many places in the literature (e.g., [5-9]), while mathematical descriptions of one or more of these microprocesses have appeared in these references as well as in [10-21]. In various places in the literature [5, 6, 9, 22-24], efforts at combining the elementary microprocesses which occur in a flotation deinking cell, into a coherent mathematical model of the overall process, have led to simple exponential-type population models for the evolution of the number of free particles in a volume element of the cell. Such models invariably tend to ignore the probability associated with the destabilization of bubble/particle aggregates due to turbulent mixing in the tank. A general transport balance model, which involves not only time variations in particle concentration due to bubble/particle aggregate formation and destruction, but also accounts for convection and diffusion processes in a unit volume of a flotation cell, has been written down, but not analyzed [9]. The model constructed in [1, 2], while not accounting for convection or diffusion processes in a typical volume element of a flotation cell, does explicitly take into account the process of bubble/particle aggregate destruction, thus leading to a more realistic logistic-type population model for the evolution of the number of free ink particles in a volume element. Before describing the macromodel and,

subsequently, introducing the new measures of flotation deinking efficiency which are the focus of the present work, we briefly summarize, in the next section, the explicit expressions for the various microprocess probabilities that we will employ.

MICROPROCESS PROBABILITIES

Probability of Capture

A particle must travel close enough to a given bubble so they will interact. A critical parameter governing this approach is R_c (Fig. 1), the radius of the streaming tube within which the particle must move so as to be intercepted by the bubble. The corresponding interception probability P_c depends on the relative sizes R_p and R_B of the particle and bubble, as well as on the assumptions one makes about the flow field in which the particle moves. Particles the size of typical ink particles in a flotation cell experience negligible inertial forces and tend, therefore, to follow the streamlines in the flow field around the bubble.

For typical ink particles St « 0.1, where St is the Stokes number given in terms of the bubble diameter d_B, the particle diameter d_p, the particle density ρ_p, the fluid viscosity μ_ℓ, and the bubble rising velocity v_B by

$$St = \frac{\rho_p d_p^2 v_B}{9\mu_\ell d_B} \equiv \frac{Re_B \rho_p d_p^2}{2\rho_\ell d_B^2} \tag{1}$$

where Re_B is the bubble Reynolds number defined by

$$Re_B = \frac{v_B d_B \rho_\ell}{\mu_\ell} \tag{2}$$

The values of the parameters St, Re_B, and C_B, where C_B gauges the degree of bubble retardation resulting from having the surface of the bubble covered by surfactant (C_B = 1 corresponding to a completely retarded bubble), are critical to determining $P_c = (R_c/R_B)^2$, the ratio of the number of particles with $R_p < R_B$ which encounter a bubble per unit time to the number of particles that approach a bubble in a streaming tube with cross-sectional area πR_c^2. By considering only the long-range hydrodynamic forces which act on a particle as it approaches a bubble (i.e., the drag, gravitational, and buoyancy forces), a system of equations (see [5]) with associated initial conditions may be written down for the velocity components of the particle whose structure depends in a crucial manner on the nature of the velocity field of the liquid in a neighborhood of the bubble. For flotation machines which are used in practice, Re_B is thought to be in the range $1 < Re_B < 100$. For this bubble Reynolds number range, a Stokes number St « 0.1, and the assumption of a rigid bubble surface, several authors ([13, 14, 16, 17]) have solved the aforementioned initial-value problem (for the velocity components of the particle) and determined that

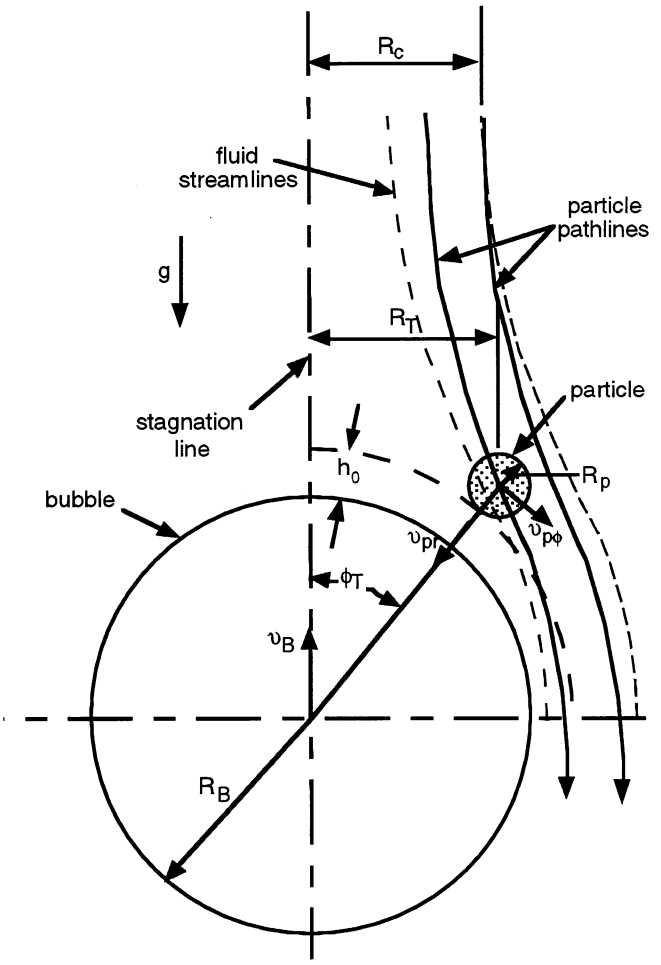

Fig. 1. A particle in streaming tube R_c intercepting an air bubble at angle ϕ_T.

$$P_c = \left[\frac{3}{2} + \frac{4Re_B^{0.72}}{15}\right]\left(\frac{R_p}{R_B}\right)^2 \tag{3}$$

The microprocess probability (of interception) given by Eq. (3) is believed to be valid for bubble sizes up to 1 mm and particle sizes up to 100 μm and will be used in this paper. Although the predictions that follow go beyond the bubble and particle ranges mentioned above, the resulting trends outside the bubble and particle size ranges are, in general, consistent with those within the range of applicability of Eq. (3), and as a first approximation, Eq. (3) will be applied over the entire bubble and particle radii considered in this study.

Probability of Adhesion by Sliding

The second microprocess, which is fundamental to the global flotation deinking process, is the sliding of a particle, which has been intercepted by a bubble at touching angle ϕ_T (see Fig. 1), along the surface of the thin liquid film which surrounds the bubble. This sliding process subjects the film to a weak surface deformation which tends to thin the film out and which may, therefore, lead to film rupture. For 'adhesion by sliding' to occur, the contact time of the particle with the liquid film must be greater than the induction (drainage) time of the film up to the point of rupture. To study this problem one must, therefore, model the motion of a particle, as it moves over the surface of the disjoining film between the bubble and the particle, so as to be able to predict the film thickness h as a function of the position angle ϕ of the particle. Note that both h and ϕ vary with the time t and that $\phi(0) = \phi_T$. It has been common in the literature to make the following assumptions in modeling the particle motion during the sliding process: (i) the particles move in a quasistationary manner on an almost circular path along the bubble surface, (ii) the sliding path L » h and dL/dt > dh/dt, (iii) for $0 < \phi < \pi/2$, the influence of the flow boundary layer is negligible, and (iv) as in the computation of P_c, the tangential component of the fluid velocity field may be modeled by the intermediate flow of Yoon and Luttrell [13].

The sliding motion of an ink particle is governed by a force balance which includes the following components: the resistive force generated during the drainage of the liquid film surrounding the bubble surface, the (apparent) weight of the particle, the centrifugal force acting on the sliding particle, the flow force which acts on the sliding particle close to the bubble wall, the lift force acting on the particle, and the drag force acting on the particle (which is strongly dependent on the flow field about the bubble and the degree of bubble surface retardation). From the force balance, a system of ordinary differential equations can be written in terms of (ϕ,h) which govern the variation of the disjoining film thickness with respect to the position of the (sliding) particle and has the initial condition $h(\phi_T) = h_0$. If h_{crit} denotes the critical thickness that the film must thin down to in order for rupture to occur, then the critical position angle ϕ^*_{crit} is defined to be the largest value of ϕ_T (<90°) for which $h = h_{crit}$ will be achieved at a position angle ϕ_{crit} such that $\phi_T < \phi_{crit} < \pi/2$; specifically,

$$\phi^*_{crit} = \max\{\phi_T = \phi(0) | h_{crit} = h(\phi_{crit}), \text{ for some } \phi_{crit},\ \phi_T \le \phi_{crit} < \pi/2\} \quad (4)$$

Figure 2 depicts the relationship that exists among ϕ_T, h_{crit}, and ϕ^*_{crit}.

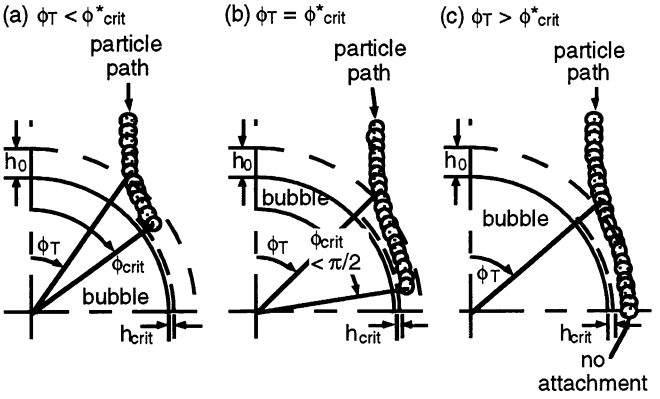

Fig. 2. Schematic representation of the relationship between ϕ_T, h_{crit}, and ϕ^*_{crit}.

The probability, P_{asl}, of adhesion by sliding is now defined to be [6]

$$P_{asl} = \sin^2 \phi^*_{crit} \quad (5)$$

The critical position angle ϕ^*_{crit} is thought to be a complex function of the system parameters (i.e., R_B, R_p, ε, etc.) that may be determined only by numerically solving the system of ordinary differential equations which govern the adhesion by sliding process [6]. As a first approximation in this model, we assume ϕ^*_{crit} to be independent of the system parameters, an assumption we will relax in future studies.

Probability of Three-Phase Contact

Once the thin film surrounding a bubble has ruptured, a sufficiently large three-phase contact (TPC) between the film, particle, and bubble has to be formed in a sufficiently short time span τ_{tpc} to provide a strong enough force of attachment to prevent the bubble/particle aggregate from immediately separating. In fact, if τ_v denotes the average lifetime for turbulent vortices within the flotation cell, then we must have $\tau_{tpc} < \tau_v$. Schulze [6] has used an exponential distribution of the approximate form

$$P_{tpc} \cong 1 - \exp\left(-\frac{\tau_v}{\tau_{tpc}}\right) \quad (6)$$

for the probability of extension of the three-phase contact, P_{tpc}. However, it is known that to within (about) 1%, $P_{tpc} = 1$ over a wide range of particle sizes [6]. We will make this same assumption in the model described in this work and, therefore, P_{tpc} will not enter into the structure of the relevant kinetic constants in the model.

Probability of Stability

The attachment that forms between a particle and a bubble must be stronger than the sum of all those external forces that act on the aggregate so as to destabilize it, otherwise the bubble/particle aggregate will not remain a stable entity on its journey to the froth layer in the flotation cell. The net detachment force which acts on an aggregate is

$$F_{det} = F_g - F_b + F_d + F_\sigma \tag{7}$$

and includes the gravitational force, F_g, the static buoyant force, F_b, the detachment force due to acceleration, F_d, and the capillary pressure force, F_σ. On the other hand, the sum of the attachment forces is given by

$$F_{ad} = F_{ca} + F_{hyd} \tag{8}$$

where F_{ca} is the capillary force and F_{hyd} is the hydrostatic pressure force. A complete description of these forces may be found in [1].

The stability of bubble/particle aggregates is then characterized by the following dimensionless similarity parameter, with $F_{hyd} \approx 0$ and F_{ca} replaced by the maximum capillary force F_{cam} [6], and is analogous to the Bond number

$$Bo' = \frac{F_{detachment}}{F_{attachment}} \tag{9}$$

where

$$F_{detachment} = 4R_p^2\left(\Delta\rho_p g + \frac{1.9\rho_p \varepsilon^{2/3}}{(R_p + R_B)^{1/3}}\right) + 3R_p\left(\frac{2\sigma}{R_B} - 2R_B\rho_\ell g\right)\sin^2\left(\pi - \frac{\theta}{2}\right) \tag{10}$$

and

$$F_{attachment} = \left|6\sigma \sin\left(\pi - \frac{\theta}{2}\right)\sin\left(\pi + \frac{\theta}{2}\right)\right| \tag{11}$$

In Eqs. (10) and (11), $\Delta\rho_p = \rho_p - \rho_\ell$, with ρ_p and ρ_ℓ the bubble and liquid density, respectively, g is the acceleration due to gravity, ε is the turbulent energy density, σ is the surface tension, and θ is the contact angle. As cited in Schulze [6], taking into account the experimental results of Plate [25], a reasonable form for P_{stab} is

$$P_{stab} = 1 - \exp\left(1 - \frac{1}{Bo'}\right) \tag{12}$$

THE KINETIC MODEL

In the kinetic (or population growth) model formulated in [1, 2], the following notation was used: $n_p(t)$ is the total number of ink particles in the volume element V_f at time t, with $n_p^f(t)$ and $n_p^a(t)$, respectively, the numbers of free and attached ink particles in V_f, while $n_B(t)$ is the total number of bubbles in the volume element V_f at time t, with $n_B^f(t)$ and $n_B^a(t)$, respectively, the numbers of free and attached bubbles in V_f. It is assumed that n_p and n_B are both time-independent, so that the model does not account for convection and/or diffusion of particles and/or bubbles into or out of V_f. In the initial model treated in [1, 2], it was also assumed that $n_p^a(t) = n_B^a(t)$, a condition which, along with several others, will be relaxed in future work. We now define

$$\gamma(t) = n_p^f(t)/n_p, t > 0 \tag{13}$$

as the ratio of free particles in V_f to the total number of particles in V_f. The goal of the kinetic model is to produce an evolution equation which can be used to study the behavior of $\gamma(t)$ for large time, as well as the dependence of $\gamma(t)$ on fundamental performance parameters associated with the microprocesses taking place in the flotation cell.

The kinetic equation constructed in [1, 2] has the form

$$\frac{dn_p^f}{dt} = -k_1 n_p^f n_B^f + k_2 n_B^a \tag{14}$$

The first term on the right-hand side represents the overall probability that a free particle will successfully attach to a bubble that is initially free of particles. The second term is a measure of the probability that a bubble/particle aggregate will become unstable and split to yield a "new" free particle. This term has not been explicitly included in previous flotation models (i.e., [5, 6, 9, 22-24]. The kinetic constants k_1 and k_2 are positive numbers described by the following relationships:

$$k_1 = ZP_cP_{asl}P_{tpc}P_{stab} \tag{15}$$

$$k_2 = P_{destab} = 1 - P_{stab} \tag{16}$$

In Eq. (15), Z is the collision frequency which we will take to have the form implied by the work of Liepe and Möckel [20], namely,

$$Z = 2^{7/9}\frac{5}{3}n_p n_B\left(\frac{\varepsilon^{4/9}}{\nu_\ell^{1/3}\rho_\ell^{2/3}}\right)\left(R_p + R_B\right)^2 \times\left(R_p^{14/9}\Delta\rho_p^{4/3} + R_B^{14/9}\Delta\rho_B^{4/3}\right)^{1/2} \quad (17)$$

where ν_ℓ is the (fluid) kinematic viscosity and $\Delta\rho_B = \rho_B - \rho_\ell$. Using the relations $n_B^f = n_B - n_B^a$, $n_p^a = n_p - n_p^f$, and $n_B^a = n_p^a$ in Eq. (14), as well as the definition of $\gamma(t)$, we are led to the equation that describes how the ratio of free particles in a flotation cell to the total number of particles in the cell varies with time

$$\frac{d\gamma}{dt} = -k_1 n_p \gamma^2(t) + \left[k_1\left(n_p - n_B\right) - k_2\right]\gamma(t) + k_2 \quad (18)$$

with initial condition $\gamma(0) = n_p^f(0)/n_p$ at t = 0. The solution of Eq. (18) results in

$$\gamma(t) \equiv \frac{n_p^f(t)}{n_p} = \mu\left[\frac{1+\beta_o^{-1}e^{-2\mu A t}}{1-\beta_o^{-1}e^{-2\mu A t}}\right] - \left[\frac{(n_B - n_p)k_1 + k_2}{2k_1 k_2}\right] \quad (19)$$

where

$$\mu = \sqrt{\frac{B^2}{4A^2} + \frac{k_2}{n_p k_1}} \quad (20)$$

$$A = n_p k_1 \quad (21)$$

$$B = (n_p - n_B)k_1 - k_2 \quad (22)$$

$$\beta_o = \frac{y_o - \mu}{y_o + \mu} \quad (23)$$

$$y_o = \frac{(n_p - n_B)k_1 - k_2}{2n_p k_1} - \frac{n_p^f(0)}{n_p} \quad (24)$$

Hence, the solution of Eq. (14) can be presented in terms of the governing system parameters (i.e., R_B, R_p, ρ_p, θ, ε, etc.).

FLOTATION CELL PERFORMANCE MEASURES

Flotation cell performance can be investigated by defining the flotation efficiency at any given time from the solution of Eq. (14) to be

$$\mathfrak{I}_e(t) = 1 - \gamma(t) = 1 - \frac{n_p^f(t)}{n_p} \quad (25)$$

Two additional measures of flotation cell performance can be ascertained from the solution of the model equation. Flotation cell efficiency can be predicted for a fixed time period, t', by

$$\mathfrak{I}_e(t = t') \equiv 1 - \gamma(t') = 1 - \left\{\mu\left[\frac{1+\beta_o^{-1}e^{-2\mu A t'}}{1-\beta_o^{-1}e^{-2\mu A t'}}\right] - \left[\frac{(n_B - n_p)k_1 + k_2}{2k_1 k_2}\right]\right\} \quad (26)$$

Alternatively, the time t* is defined as the time period required to reduce the number of free particles in a representative unit volume by a specific amount γ^*, where γ^* is a specified fraction of $\gamma(0) = n_p^f(0)/n_p$. It may be shown that

$$t^* = \frac{1}{2\mu A}\ell n\left\{\frac{1}{\beta_o}\left[\frac{\frac{1}{\mu}\left(\gamma^* + \frac{|B|}{2A}\right)+1}{\frac{1}{\mu}\left(\gamma^* + \frac{|B|}{2A}\right)-1}\right]\right\} \quad (27)$$

For example, the time required to reduce the initial number of free (ink) particles in a representative unit volume by a factor of two (i.e., $\gamma^* = \gamma(0)/2 = n_p^f(0)/(2n_p)$) can be expressed as

$$t^* = t_{1/2} = \frac{1}{2\mu A}\ell n\left\{\frac{1}{\beta_o}\left[\frac{\frac{1}{\mu}\left(\frac{1}{2}\frac{n_p^f(0)}{n_p} + \frac{|B|}{2A}\right)+1}{\frac{1}{\mu}\left(\frac{1}{2}\frac{n_p^f(0)}{n_p} + \frac{|B|}{2A}\right)-1}\right]\right\} \quad (28)$$

These three measures of flotation cell performance will be addressed below.

MODEL CONDITIONS

Recall that the kinetic constants k_1 and k_2 are expressed in terms of the probabilities of the various flotation microprocesses, which are themselves functions of system parameters such as bubble size, particle size, contact angle, surface tension, etc. Therefore, flotation cell performance can be predicted if appropriate values of the system parameters are identified.

One difficulty in identifying appropriate values for the system parameters is that the many variables within the microprocess equations may, themselves, be related to each other in a complex fashion. For example, the bubble rise velocity (terminal rise velocity) is a balance between the buoyant and drag forces acting on the bubble, and these

forces are related to the bubble radius, fluid flow field, and fluid properties. However, the bubble rise velocity is a very complex function of bubble equivalent diameter as well as contaminant level (surface tension) in a gas/water system [26], and this relationship is unknown for a gas/water/fiber system. Since a flotation cell will typically have surfactants and other contaminants in the system, as a first approximation we assume the bubble rise velocity (υ_B) will be constant over a wide range of bubble diameters and it will be substantially below that of pure water with υ_B = constant = 10 cm/s. We also assume the liquid properties are constant and correspond to those of water.

Additionally, it has been shown that bubble diameter can be related to surface tension and turbulent energy density [27-29], and following Schulze [12] employ

$$\sigma = (2R_B)^{5/3} \varepsilon^{2/3} \rho_\ell \tag{29}$$

A literature search was also conducted to identify experimental and theoretical ranges of the various system parameters utilized by other investigators in their flotation separation studies [6, 8, 11, 12, 19, 21, 30-41]. The maximum and minimum values identified in this search are outlined in Table 1. From these conditions, appropriate parametric ranges were selected to determine how flotation efficiency varies over these ranges, while assuming at time t = 0, $n_p^f(0) = n_p$.

Another complication with flotation efficiency predictions is that (as shown in Table 1) it is a function of many variables. In this study, variables that were fixed were kept at their "standard" conditions identified in Table 1, unless otherwise noted. These conditions refer to reasonable values identified by previous investigators [6, 8, 11, 12, 19, 21, 30-41]. To maximize the usefulness of the predictions, selected results are reported for one parameter that has been varied over its entire range, while another variable is fixed at

Table 1: Parametric ranges of the various flotation parameters addressed in the literature and utilized in this study [6, 8, 11, 12, 19, 21, 30-41].

Parameter	Minimum Value Used in the Literature	Maximum Value Used in the Literature	Parametric Range Utilized in this Study	"Standard" Conditions	Calculations Performed At Selected Values
R_p (μm)	1	600	1-500	50	1, 10, 50, 100, 200, 300, 500
R_B (mm)	0.15	2	0.1-5.0	0.5	0.1, 0.3, 0.5, 0.7, 1.0, 3.0, 5.0
ρ_p (g/cm^3)	1	7.5	1.0-3.0	1.3	1.0, 1.1, 1.3, 1.5, 2.0, 3.0
ρ_ℓ (g/cm^3)	1	1	–	1	1
υ_B (cm/s)	1.25	30	–	10	10
μ_ℓ (cP)	1	1	–	1	1
ε (W/kg)	1	130	1-400	10	1, 10, 50, 100, 200, 400
σ (dynes/cm)	35	73	Eq. (29)	Eq. (29)	Eq. (29)
θ (deg)	5	105	5-120	60	20, 40, 60, 80, 100, 120
ϕ^*_{crit} (deg)	33	72	5-85	60	20, 40, 60, 80
n_B	–	–	100-10000	1000	200, 500, 1000, 5000, 10000
n_p	–	–	1-1000	100	1, 10, 50, 100, 500, 975

selected values that cover its parametric range. These values are identified in the last column of Table 1 as "Calculations Performed At Selected Values." All the predictions in this report were calculated at the selected values, but some figures do not show results for a given value because the result produced unstable bubble/particle aggregates (i.e., $P_{stab} < 0$). When this occurred, the selected parameter was omitted from the figure. For example, when calculations were performed for selected particle radii, predictions with R_p = 500 μm typically produced $P_{stab} < 0$ (which depends on R_B) and these results are not shown in the figures.

RESULTS

Utilizing the values and ranges outlined in Table 1 for the parameters required to solve the model equation, flotation cell performance, based upon our first-generation model (Eq. (14) with solution Eq. (19)), is predicted and discussed below. We will address three performance measures. First, flotation efficiency as a function of time will be presented for selected values of each parameter, while holding all other parameters fixed at their standard conditions. Then flotation efficiency at t = 1 second will be discussed and displayed as a function of one parameter while choosing selected values of another parameter, with the remaining parameters fixed at their standard conditions. Finally, the time required to reduce the number of free particles in a representative unit volume by a factor of two will be presented.

Flotation Efficiency as a Function of Time

Selected bubble radii encompassing the entire range of interest (0.1 mm ≤ R_B ≤ 5.0 mm) were used to generate predictions of flotation efficiency as a function of time. As shown in Fig. 3, for the given fixed conditions, increasing the flotation time in a representative unit volume increases flotation efficiency until an asymptotic limit is reached, which is very low for R_B = 0.1 mm (asymptotic limit of $\mathfrak{I}_e(t) \approx 0.06$), but increases as bubble radius increases. The low asymptotic limit of the predictions with R_B = 0.1 mm is a direct result of including the second term in Eq. (14). At these small bubble radii, not many stable bubble/particle aggregates form. An asymptotic limit of $\mathfrak{I}_e(t) \approx 1.0$ is reached when $R_B \geq 0.5$ mm, and larger bubble radii reduce the time period necessary to reach this limit.

The effect particle radius (1 μm ≤ R_p ≤ 500 μm) has on flotation efficiency as a function of time is shown in Fig. 4. Particle radii greater than 200 μm (i.e., calculations at R_p = 300 and 500 μm) are not shown in Fig. 4 because at the larger particle radii, the correlation for P_{stab} results in $P_{stab} <$ 0 for the given conditions, which implies the bubble and particle will not form a stable aggregate under these conditions. When R_p = 200 μm, flotation efficiency is very

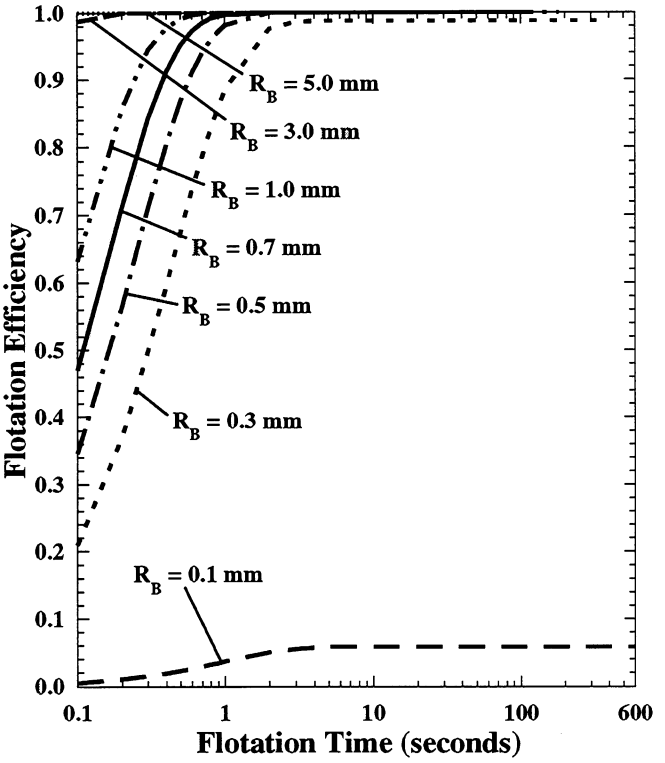

Fig. 3. Flotation efficiency as a function of time ($\mathfrak{I}_e(t)$) for selected bubble radii, R_B. All other parameters are at the standard conditions: R_p = 50 μm, ρ_p = 1.3 g/cm^3, ε = 10 W/kg, θ = 60°, ϕ^*_{crit} = 60°, n_B = 1000, and n_p = 100.

high at t = 0.1 sec, but asymptotes to a value less than 1. As the particle radius decreases, a longer time period is required for the flotation efficiency to asymptote to a constant value, which approaches 1. Even when R_p = 1 μm, flotation efficiency is predicted to asymptote to 1, but particles this small are typically not removed in conventional flotation cells [3, 4]. This apparent discrepancy between the model and actual operation can be explained by focusing on how long the actual required time period is for the efficiency to asymptote to 1 for R_p = 1 μm – well over 6000 seconds. Hence, a particle with R_p = 1 μm *must* remain in the unit volume for almost *1.7 hours* to eventually collide with and attach to a bubble. This is highly unlikely in actual flotation cell operation because the stock will typically remain in a unit volume for a much shorter time period, which may even be less than 1 second, depending on the definition of a representative unit volume, which may be large or very small. For example, when t ≈ 100 seconds, $\mathfrak{I}_e(t) \approx 0.12$ for R_p = 1 μm, which is a very poor removal efficiency, and when t ≈ 1 second for the same conditions, $\mathfrak{I}_e(t) \approx 0$.

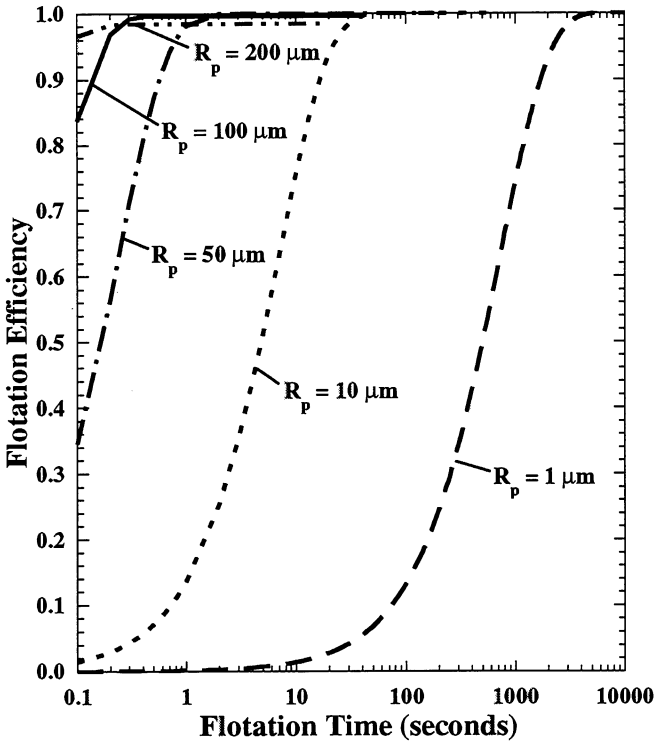

Fig. 4. Flotation efficiency as a function of time ($\Im_e(t)$) for selected particle radii, R_p. All other parameters are at the standard conditions: R_B = 0.5 mm, ρ_p = 1.3 g/cm^3, ε = 10 W/kg, θ = 60°, ϕ^*_{crit} = 60°, n_B = 1000, and n_p = 100.

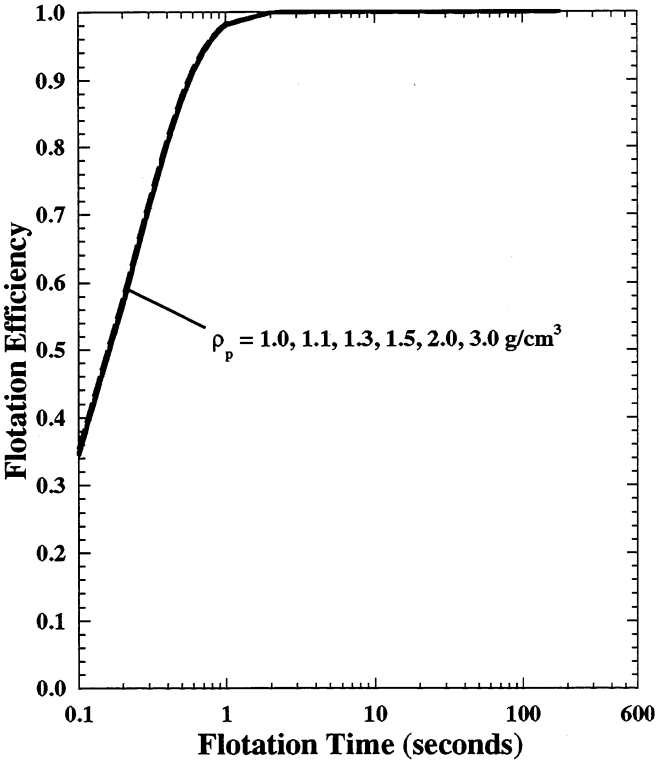

Fig. 5. Flotation efficiency as a function of time ($\Im_e(t)$) for selected particle densities, ρ_p. All other parameters are at the standard conditions: R_B = 0.5 mm, R_p = 50 μm, ε = 10 W/kg, θ = 60°, ϕ^*_{crit} = 60°, n_B = 1000, and n_p = 100.

Not all variations in the independent variables result in large fluctuations in the predicted efficiency as a function of time. For example, the influence particle density has on the predicted flotation efficiency is shown in Fig. 5. The flotation fluid density is assumed to correspond to that of water ($\rho_\ell \approx 1.0$ g/cm^3), so any freely moving contaminant particle with a lower density and a long enough retention time will naturally float to the surface. Particle densities of interest in this study encompass 1.0 g/cm^3 $\leq \rho_p \leq$ 3.0 g/cm^3, which covers the density range of many inks and toners used in the industry [42, 43]. As displayed in Fig. 5, the particle density in this range has a negligible effect on flotation efficiency as a function of time when the remaining parameters are fixed at their standard conditions.

Additional calculations were performed to investigate flotation efficiency as a function of time for the remaining independent parameters. Results show that flotation efficiency will increase as flotation time increases and will asymptote to a constant value given a long enough flotation time. In general, for the given conditions addressed in this study, varying R_B, R_p, ε, ϕ^*_{crit}, n_B, or n_p, while holding all other parameters fixed, produced families of similarly-shaped curves. Altering ρ_p or θ over the ranges considered in this study, while holding all other parameters fixed, resulted in no significant effect on flotation efficiency as a function of time.

Flotation Efficiency at t = 1 Second

Recognizing that in actual flotation deinking operations a particle and/or bubble may remain in a representative unit volume only for a short period of time, insight into which parameters affect particle removal rate may be gained by fixing the flotation time period and determining the efficiency under these conditions ($\Im_e(t=t')$). Equation (26) is utilized in these calculations and t' is fixed at t = 1 second. Therefore, $\Im_e(t=t') \equiv \Im_e(t=1)$. Figures of $\Im_e(t=1)$ were generated over the range of independent parameters for selected values of another parameter, while holding the remaining six parameters fixed, with selected results presented here.

Although the efficiency for R_p = 1 μm is shown to asymptote to 1 given a long enough flotation time, a

flotation time of t = 1 second reveals that these particles are not removed very effectively over the entire range of bubble radii considered (Fig. 6). Increasing R_p to R_p = 10 μm still predicts poor removal efficiencies at small bubble radii, but $\mathfrak{I}_e(t=1)$ improves as the bubble radius increases. Even better performance over the entire bubble radii range is predicted when R_p = 50 μm with $\mathfrak{I}_e(t=1) \approx 1$ for $R_B \gtrsim 0.7$ mm. Further increases in the particle radius still produce $\mathfrak{I}_e(t=1) = 1$ when $R_B \gtrsim 0.7$. However, the predicted efficiency drops drastically toward zero when $R_B < 0.7$ mm, with $\mathfrak{I}_e(t=1) \approx 0$ at $R_B \approx 0.2$, 0.37, and 0.58 mm for R_p = 100, 200, and 300 μm, respectively, because $P_{stab} < 0$ for smaller values of R_B. This trend is revealed in Fig. 6 by the abrupt termination of the curves for the various values of R_p as R_B is reduced. The efficiency at t = 1 second does go to zero in a continuous fashion at a value of R_B slightly less than the last value plotted, but the exact zero location for each curve was not determined because the curves are highly sensitive to the selected parametric values. Calculations performed at R_p = 500 μm provide no stable bubble/particle aggregate for removal under the given fixed conditions.

For a flotation efficiency at t = 1 second, small particles are not removed very effectively, if at all. Increasing the particle radius results in an increase in $\mathfrak{I}_e(t=1)$ until a maximum is reached over a given particle size range, which depends on the given conditions, then the efficiency rapidly declines toward zero because the bubble/particle aggregate becomes unstable. These trends are clearly displayed in Fig. 7 over the range of selected bubble radii. When R_B = 0.1 mm, a poor removal efficiency results over the entire particle radius range with a maximum occurring at $R_p \approx 35$ μm where $\mathfrak{I}_e(t=1) \approx 0.15$. Increasing the bubble radius increases $\mathfrak{I}_e(t=1)$ and increases the particle radius range at which the maximum in $\mathfrak{I}_e(t=1)$ is observed. The shape of these curves is similar to those typically presented when flotation efficiency is plotted as a function of particle size, where flotation is performed for a given time period [3, 40].

Similar curves result from variation of the other parameters. Of special interest is the fact that the increase in efficiency is independent of particle density and contact angle, but the decline in efficiency is influenced by variations in these parameters. For example, as shown in Fig. 8, particle

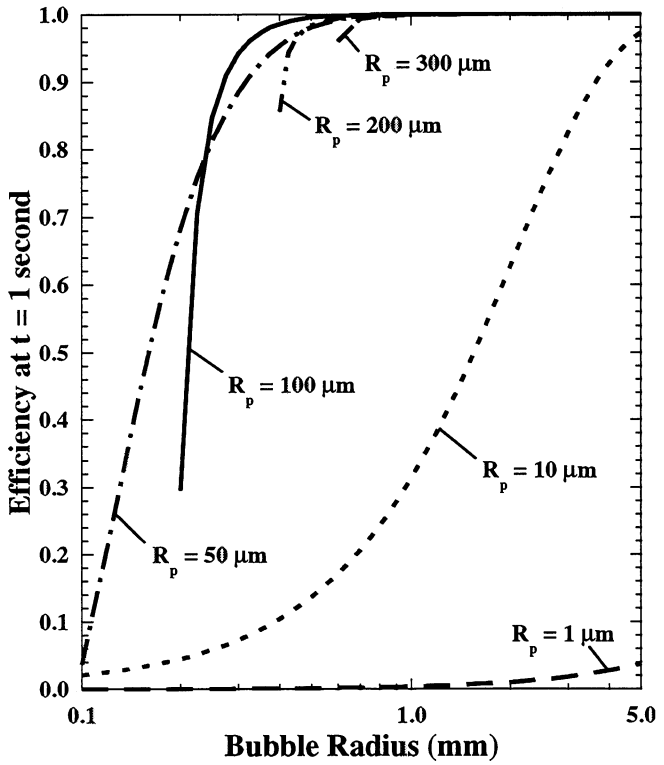

Fig. 6. Flotation efficiency at t = 1 second ($\mathfrak{I}_e(t=1)$) as a function of bubble radius, R_B, for selected particle radii, R_p. All other parameters are at the standard conditions: ρ_p = 1.3 g/cm^3, ε = 10 W/kg, θ = 60°, ϕ^*_{crit} = 60°, n_B = 1000, and n_p = 100.

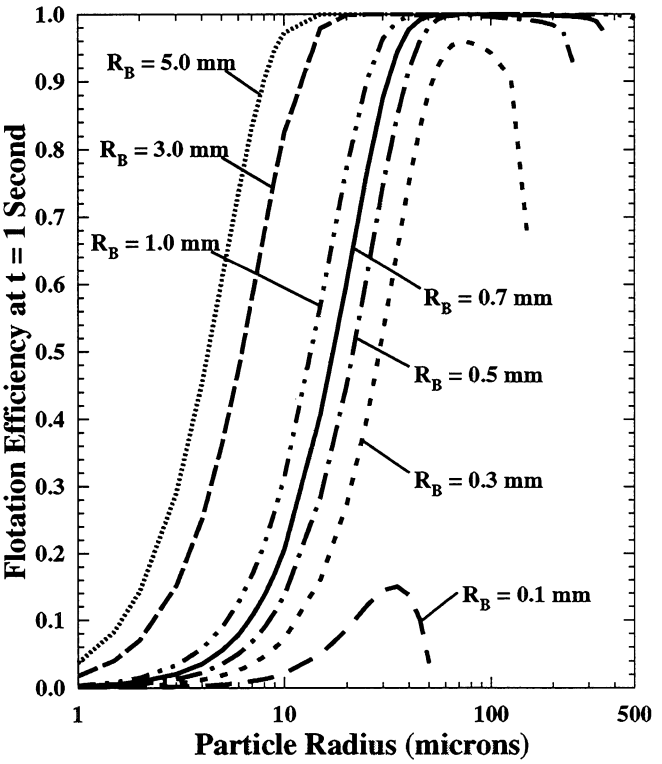

Fig. 7. Flotation efficiency at t = 1 second ($\mathfrak{I}_e(t=1)$) as a function of particle radius, R_p, for selected bubble radii, R_B. All other parameters are at the standard conditions: ρ_p = 1.3 g/cm^3, ε = 10 W/kg, θ = 60°, ϕ^*_{crit} = 60°, n_B = 1000, and n_p = 100.

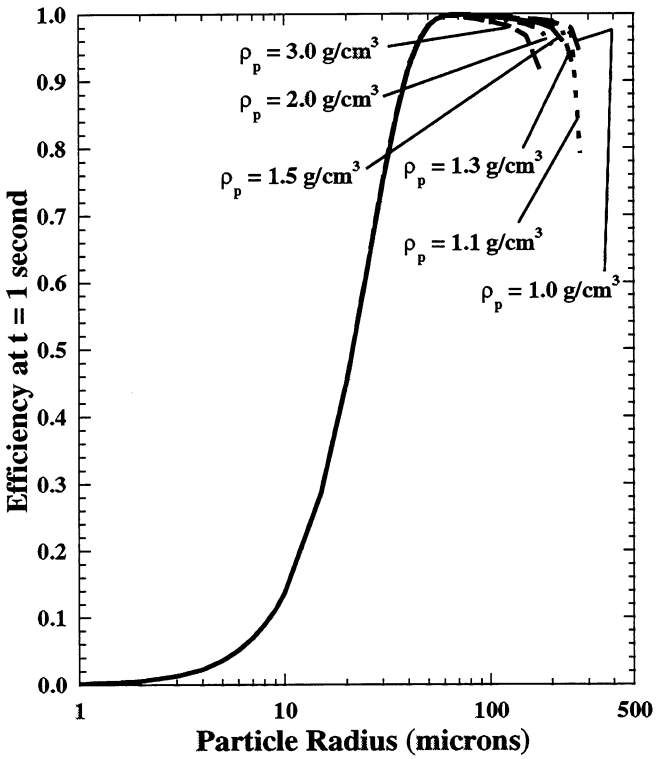

Fig. 8. Flotation efficiency at t = 1 second ($\mathfrak{I}_e(t=1)$) as a function of particle radius, R_p, for selected particle densities, ρ_p. All other parameters are at the standard conditions: R_B = 0.5 mm, ε = 10 W/kg, θ = 60°, ϕ^*_{crit} = 60°, n_B = 1000, and n_p = 100.

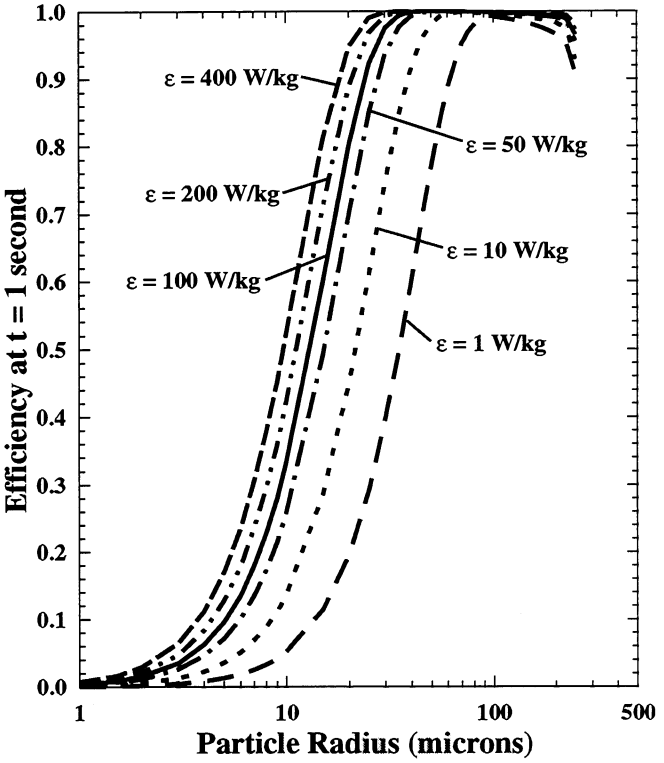

Fig. 9. Flotation efficiency at t = 1 second ($\mathfrak{I}_e(t=1)$) as a function of particle radius, R_p, for selected turbulent energy densities, ε. All other parameters are at the standard conditions: R_B = 0.5 mm, ρ_p = 1.3 g/cm^3, θ = 60°, ϕ^*_{crit} = 60°, n_B = 1000, and n_p = 100.

density does not affect the increase in $\mathfrak{I}_e(t=1)$ as R_p increases, but particles with a higher density will form an unstable bubble/particle aggregate at smaller particle radii, which causes a rapid decline in efficiency for the larger particle radii. In contrast, variations in the turbulent energy density, critical attachment angle, number of bubbles, and number of particles result in particle radius differences where the efficiency increases, but does not significantly affect the particle radius at which the efficiency drops toward zero ($R_p \approx 250$ μm). For example, this trend is shown in Fig. 9 for selected values of turbulent energy density, ε.

In general, results from calculations performed using Eq. (26) reveal that flotation efficiency after a flotation time of 1 second is sensitive to most parameters considered in this study, with increasing the respective parameter generally resulting in an increase in $\mathfrak{I}_e(t=1)$. However, when the bubble/particle aggregate becomes unstable, the efficiency drops drastically toward zero. The best examples of these trends are revealed when particle radius is varied and calculations are performed at selected bubble radii (i.e., Fig. 7).

Time Required to Reduce the Number of Free Particles by a Factor of Two

The flotation time required to reduce the number of free particles in a representative unit volume by a factor of two (Eq. (28)) – $t_{1/2}$) may be calculated to determine what parameters should be altered to reduce this time period as much as possible. Note that when $P_{stab} < 0$, $t_{1/2}$ does not have a physical meaning, therefore no value is plotted when this condition occurs. This manifests itself by curves that appear to decline sharply from large values of $t_{1/2}$ (e.g., Fig. 10) or rise abruptly toward large values of $t_{1/2}$ (e.g., Fig. 11).

Figure 10 reveals the effect bubble radius has on $t_{1/2}$ for selected particle radii, and show the general trend of a reduction in $t_{1/2}$ as R_B increases. Even when R_p = 1 μm, the number of particles in a representative unit volume can be reduced by a factor of two, but the required time period for this to occur could be as large as 4000 seconds (over 1 hour). Increasing the particle radii reduces $t_{1/2}$ by several orders of magnitude, but for given combinations of large

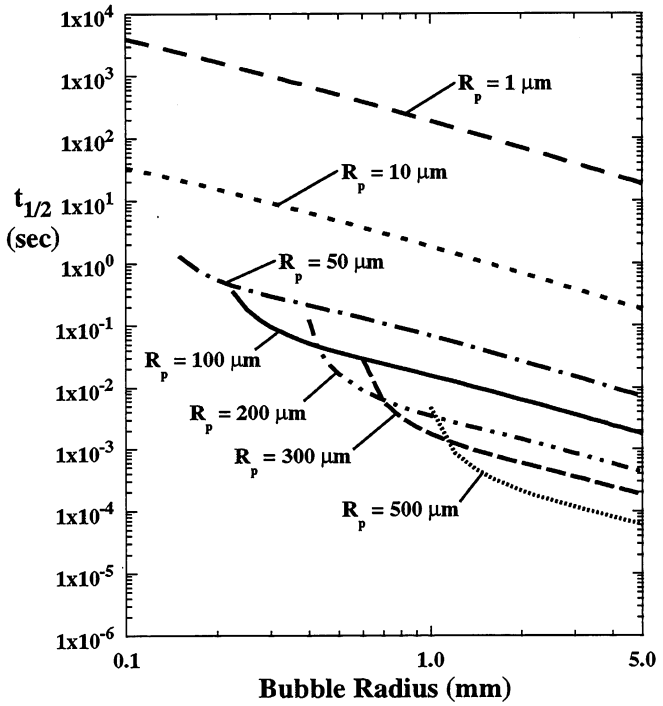

Fig. 10. Time required to reduce the number of free particles by a factor of two ($t_{1/2}$) as a function of bubble radius, R_B, for selected particle radii, R_p. All other parameters are at the standard conditions: ρ_p = 1.3 g/cm^3, ε = 10 W/kg, θ = 60°, ϕ^*_{crit} = 60°, n_B = 1000, and n_p = 100.

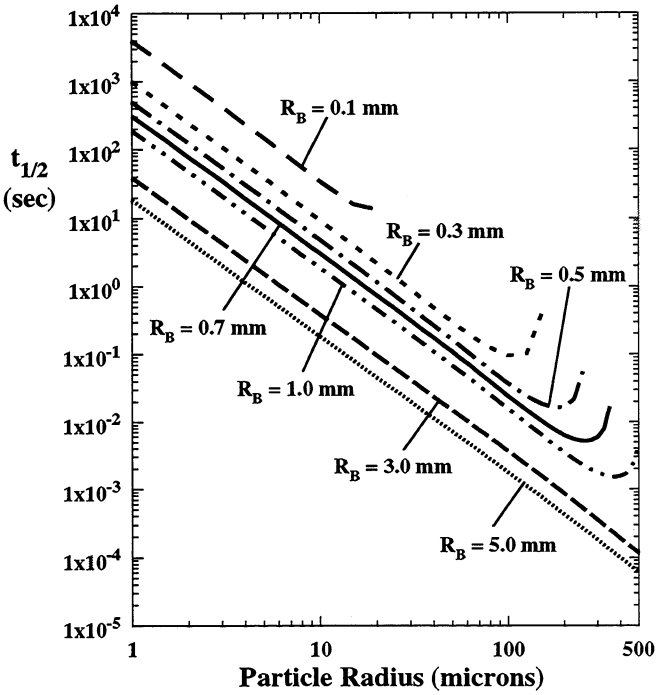

Fig. 11. Time required to reduce the number of free particles by a factor of two ($t_{1/2}$) as a function of particle radius, R_p, for selected bubble radii, R_B. All other parameters are at the standard conditions: ρ_p = 1.3 g/cm^3, ε = 10 W/kg, θ = 60°, ϕ^*_{crit} = 60°, n_B = 1000, and n_p = 100.

particles and small bubbles, $P_{stab} < 0$, and $t_{1/2}$ increases dramatically as this combination is approached when the bubble radius is reduced.

The effect particle radius has on the time required to reduce the number of free particles in a representative unit volume by a factor of two is shown in Fig. 11 for selected bubble radii. In general, $t_{1/2}$ decreases by several orders of magnitude as the particle radius increases until the particle is so large that, for the given parameters, the bubble/particle aggregate is no longer stable and, just prior to this condition, $t_{1/2}$ abruptly increases. One interesting feature of these predictions is that the decline in $t_{1/2}$, as a function of R_p, is independent of ρ_p and θ, but the increase in $t_{1/2}$ where the bubble/particle aggregate becomes unstable is not. In contrast, ε, ϕ^*_{crit}, n_B, and n_p influence the decline in $t_{1/2}$ as a function of R_p, producing families of similar curves, but the abrupt increase in $t_{1/2}$ typically occurs at $R_p \approx 250$ μm and is independent of these parameters. Finally, both effects are observed when R_B is altered (as shown in Fig. 11), indicating that bubble radius is the most influential parameter when comparing $t_{1/2}$ as a function of R_p.

CONCLUSIONS

A population balance-type model has been developed that utilizes two kinetic constants that depend on the individual microprocesses related to flotation. These microprocesses have been summarized in terms of the independent variables governing the flotation process. From the solution of the model equation, three performance parameters have been identified: (1) flotation efficiency as a function of time, (2) flotation efficiency for a given time period, and (3) the time it takes to reduce the number of free particles by a given amount.

Flotation efficiency ($\mathfrak{I}_e(t)$) will increase as flotation time increases and will asymptote to a constant value given a long enough flotation time. This may occur in time periods of less than 1 second to more than 1 hour, depending on the model parameters, with larger bubbles and particles with $R_p \approx 100$ μm providing the fastest results.

Flotation efficiency after a flotation time of 1 second ($\mathfrak{I}_e(t=1)$) is sensitive to most parameters considered in this study, with increasing the respective parameter generally

resulting in an increase in $\Im_e(t=1)$. However, when the bubble/particle aggregate becomes unstable, the efficiency drops drastically toward zero. The combined effect results in bell-shaped curves typically presented in the literature when flotation efficiency is plotted as a function of particle radius.

The time required to reduce the total number of free particles in a representative unit volume by a factor of two ($t_{1/2}$) generally decreases as the considered parameters are increased. The decrease in $t_{1/2}$ is most sensitive to bubble radius and particle radius, and variations of more than several orders of magnitude are predicted.

Finally, the model presented in this report incorporates various assumptions to reach a mathematical solution. Selected assumptions will be relaxed in future work.

REFERENCES

1. Bloom, F., and Heindel, T.J., "Mathematical Modeling of the Flotation Deinking Process," *Submitted for Publication* (1996).
2. Bloom, F., and Heindel, T.J., "A Theoretical Model of Flotation Deinking Efficiency," *Submitted for Publication* (1996).
3. Ferguson, L.D., "Flotation Deinking Technology," *1995 Deinking Short Course*, Vancouver, WA, TAPPI Press, Chapter 10 (June 4-7, 1995).
4. McCool, M.A., "Flotation Deinking," *Secondary Fiber Recycling*, R.J. Spangenberg, Ed., TAPPI Press, Atlanta, 141-162 (1993).
5. Schulze, H.J., *Physico-chemical Elementary Processes in Flotation*, Elsevier, Berlin, 1984.
6. Schulze, H.J., "Flotation as a Heterocoagulation Process: Possibilities of Calculating the Probability of Flotation," *Coagulation and Flocculation*, B. Dobias, Ed., 321-353 (1993).
7. Schulze, H.J., "The Fundamentals of Flotation Deinking in Comparison to Mineral Flotation," *1st Research Forum on Recycling*, Toronto, Ontario, 161-167 (October 29-31, 1991).
8. Schulze, H.J., "Probability of Particle Attachment on Gas Bubbles by Sliding," *Advances in Colloid and Interface Science*, **40**: 283-305 (1992).
9. Plate, H., and Schulze, H.J., "Modeling of the Overall Flotation Process Based on Physico-Chemical Microprocesses - Technique and Application," *XVII International Mineral Processing Congress*, Dresden, 365-377 (September 23-28, 1991).
10. Pan, R., Paulson, F.G., Johnson, D.A., Bousfield, D.W., and Thompson, E.V., "A Global Model for Predicting Flotation Efficiency Part I: Model Results and Experimental Studies," *TAPPI Journal*, **79**(4): 177-185 (1996).
11. Pan, R., Bousfield, D.W., and Thompson, E.V., "Modeling Particle-Bubble Dynamics and Adhesion in Air/Solid Particle/Liquid Systems," *Proceedings 1992 Pulping Conference*, Tappi Press, 941-956 (1992).
12. Schulze, H.J., "Zur Hydrodynamik der Flotations-Elementarvorgänge," *Wochenblatt Für Papierfabrikation*, **122**(5): 160, 162, 164-168 (1994).
13. Yoon, R.H., and Luttrell, G.H., "The Effect of Bubble Size on Fine Particle Flotation," *Mineral Processing and Extractive Metallurgy Review*, **5**: 101-122 (1989).
14. Dukhin, S.S., Rulev, N.N., and Dimitrov, A.S., *Koagulyastsiya i Dinamika Tonkikh Plenok*, Naukova Dumka, Kiev, 1986.
15. Derjaguin, B.V., Dukhin, S.S., and Rulev, N.N., "Thin-Film Capillary Hydrodynamic Method in the Theory of Flotation," *Colloid Journal of the USSR*, **39**(6): 926-933 (1978).
16. Derjaguin, B.V., Dukhin, S.S., and Rulev, N.N., *Microflotacija*, Chimija Moskva, 1986.
17. Ahmed, N., and Jameson, G.J., "Flotation Kinetics," *Frothing in Flotation*, J. Laskowski, Ed., Gordon and Breach, New York, 77-99 (1989).
18. Williams, M.B., and Davis, S.H., "Nonlinear Theory of Film Rupture," *Journal of Colloid and Interface Science*, **90**(1): 220-228 (1982).
19. Paulsen, F.G., Pan, R., Bousfield, D.W., and Thompson, E.V., "The Dynamics of Bubble/Particle Approach and Attachment During Flotation and the Influence of Short-Range Nonhydrodynamic Forces on Disjoining Film Rupture," *2nd Research Forum on Recycling*, Ste-Adèle, Quebec, 1-12 (October 5-7, 1993).
20. Liepe, F., and Möckel, O.H., "Untersuchengen zum Stoffvereinigen in flüssiger Phase," *Chemical Technology*, **30**: 205-209 (1976).
21. Hou, M.J., and Hui, S.H., "Interfacial Phenomena in Deinking I. Stability of Ink Particle - Air Bubble Aggregates in Flotation Deinking," *1993 Pulping Conference*, TAPPI Press, Atlanta, GA, 1125-1142 (1993).
22. Woodburn, E.T., "Mathematical Modeling of Flotation Processes," *Mineral Science and Engineering*, **2**: 3-17 (1970).

23. Sutherland, K.L., "Kinetics of the Flotation Process," *Journal of Physical Chemistry*, **52**: 394-425 (1948).

24. Dorris, G.M., and Pagé, M., "Deinking of Toner-Printed Papers. Part I: Flotation Kinetics, Froth Stability and Fibre Entrainment," *3rd Research Forum on Recycling*, Vancouver, BC, 215-225 (November 20-22, 1995).

25. Plate, H., Ph.D. thesis, ADW, UVR Freiberg/Sa. Chemnitzer Str. 40, unpublished.

26. Clift, R., Grace, J.R., and Weber, M.E., *Bubble, Drops, and Particles*, Academic Press, New York, 1978.

27. Sprow, F.B., "Distribution of Drop Sizes Produced in Turbulent Liquid-Liquid Dispersion," *Chemical Engineering Science*, **22**: 435-442 (1967).

28. Hinze, J.O., "Fundamentals of the Hydrodynamic Mechanism of Splitting Up in Dispersion Processes," *AIChE Journal*, **1**: 289 (1955).

29. Tsouris, C., and Tavlarides, L.L., "Breakage and Coalescence Models for Drops in Turbulent Dispersions," *AIChE Journal*, **40**(3): 395-406 (1994).

30. Anfruns, J.P., and Kitchener, J.A., "The Absolute Rate of Capture of Single Particles by Single Bubbles," *Flotation*, M.C. Fuerstenau, Ed., American Institute of Mining, Metallurgical, and Petroleum Engineers, Inc., New York, 625-637 (1976).

31. Dobby, G.S., and Finch, J.A., "A Model of Particle Sliding Time for Flotation Size Bubbles," *Journal of Colloid and Interface Science*, **109**(2): 493-498 (1986).

32. Nguyen-Van, A., and Kmet, S., "Collision Efficiency for Fine Mineral Particles with Single Bubble in a Countercurrent Flow Regime," *International Journal of Mineral Processing*, **35**(3/4): 205-223 (1992).

33. Nguyen-Van, A., Kmet, S., and Schulze, H.J., "Collection Events in Flotation: The Quantitative Analysis of the Particle-Bubble Collision and the Attachment of Particle onto Bubble Surface," *XIX International Mineral Processing Congress*, San Francisco, CA (October 22-27, 1995).

34. Pan, R., Paulsen, F.G., Johnson, D.A., Bousfield, D.W., and Thompson, E.V., "A Global Model for Predicting Flotation Efficiencies: Model Results and Experimental Studies," *1993 Pulping Conference Proceedings*, TAPPI Press, 1155-1164 (1993).

35. Schulze, H.J., "Comparison of the Elementary Steps of Particle/Bubble Interaction in Mineral and Deinking Flotation," *8th International Conference on Colloid and Surface Science*, (February, 1994).

36. Schulze, H.J., Radoev, B., Geidel, T., Stechemesser, H., and Töpfer, E., "Investigation of the Collision Process Between Particles and Gas Bubbles in Flotation - A Theoretical Analysis," *International Journal of Mineral Processing*, **27**(3/4): 263-278 (1989).

37. Schulze, H.J., Wahl, B., and Gottschalk, G., "Determination of Adhesive Strength of Particles within the Liquid/Gas Interface in Flotation by Means of a Centrifuge Method," *Journal of Colloid and Interface Science*, **128**(1): 57-65 (1989).

38. Stratton, R.A., "The Surface Chemistry of Flotation of Stickies and Laser Printed Inks," IPST, Atlanta, GA, Technical Paper Series, 397, (September 1991).

39. Stratton, R.A., "Separation by Flotation of Contaminants from Recycled Fiber," *1992 Contaminant Problems Seminar*, Cincinnati, OH, TAPPI Press, 13-21 (April 28-30, 1992).

40. Vidotti, R.M., Johnson, D.A., and Thompson, E.V., "Hydrodynamic Particle Volume and Its Relationship to Mixed Office Waste Paper Flotation Efficiency, Part 1," *1995 Pulping Conference*, TAPPI Press, Atlanta, 203-213 (1995).

41. Vinke, H., Hamersma, P.J., and Fortuin, J.M.H., "Particle-to-Bubble Adhesion in Gas/Liquid/Solid Slurries," *AIChE Journal*, **37**(12): 1801-1809 (1991).

42. Merriman, K., "Cleaning for Contaminant Removal in Recycled-Fiber Systems," *Secondary Fiber Recycling*, R.J. Spangenberg, Ed., TAPPI Press, Atlanta, 101-123 (1993).

43. Vidotti, R.M., Johnson, D.A., and Thompson, E.V., "Repulping and Flotation Studies of Photocopied and Laser-Printed Office Waste Paper: Part I: Repulping and Image Analysis," *Progress in Paper Recycling*, **2**(4): 30-39 (1993).

ACKNOWLEDGMENT

The work described in this paper was funded by the Member Companies of the Institute of Paper Science and Technology. Their continued support is gratefully acknowledged.